Thrombus Inducing Property of Atomically Thin Graphene Oxide Sheets

Sunil K. Singh,[†] Manoj K. Singh,[‡] Manasa K. Nayak,[†] Sharda Kumari,[†] Siddhartha Shrivastava,[†] José J. A. Grácio,[‡] and Debabrata Dash[†,*]

[†]Department of Biochemistry, Institute of Medical Sciences, Banaras Hindu University, Varanasi 221005, India, and [‡]Center for Mechanical Technology & Automation, Department of Mechanical Engineering, University of Aveiro, Aveiro 3810-193, Portugal

ABSTRACT Graphene oxide (GO), the new two-dimensional carbon nanomaterial, is extensively investigated for potential biomedical applications. Thus, it is pertinent to critically evaluate its untoward effects on physiology of tissue systems including blood platelets, the cells responsible for maintenance of hemostasis and thrombus formation. Here we report for the first time that atomically thin GO sheets elicited strong aggregatory response in platelets through activation of Src kinases and release of calcium from intracellular stores. Compounding this, intravenous administration of GO was found to induce extensive pulmonary thromboembolism in mice. Prothrombotic character of GO was dependent on surface charge distribution as reduced GO (RGO) was significantly less effective in aggregating platelets. Our findings raise a concern on putative biomedical applications of GO in the form of diagnostic and therapeutic tools where its prothrombotic property should be carefully investigated.

KEYWORDS: graphene oxide · thrombus · Src kinases · intracellular calcium · surface charge distribution · thromboembolism

Carbon-based nanomaterials have been extensively explored because of their remarkable physical, chemical, and biological properties.[1−5] Recently, graphene oxide (GO), a heavily oxygenated graphene derivative having high stability in aqueous dispersion, has attracted enormous interest among biomedical researchers.[6−9] Potential applications of GO have been suggested in areas of cellular imaging and drug delivery.[6,10,11] Further, recent reports have implicated GO with antibacterial[12,13] and antitumor therapeutic strategies.[14] Biocompatibility of GO nanosheets opens up possibilities for their direct application in biological devices, clinical diagnosis, and electrochemistry.[15] Growing use of GO has thus aroused the need to establish a paradigm for accurately predicting its cytotoxicity in biological system.

Literature is stuffed with reports that carbon nanomaterials can cause inflammation, fibrosis, and epithelioid granulomas in lungs,[16−20] cellular cytoxicity,[21] and cardiovascular abnormalities.[22,23] Carbon nanotubes have also been shown to activate transcription factor nuclear factor-κB in human keratinocytes[24] and platelet activity.[23,25,26] In view of growing application of GO, it is of paramount importance to determine its effect on various blood components including platelets, which has the central role in pathogenesis of life-threatening conditions of stroke and myocardial infarction.[27−29] Here we report for the first time that GO can potentially activate platelets and induce integrin $\alpha_{IIb}\beta_3$-mediated aggregation and adhesion of cells to immobilized fibrinogen. Platelet aggregation in the presence of GO was associated with significant phosphorylation of platelet proteins on tyrosine residues, attributable to upregulation of Src kinase activity and release of calcium from intracellular stores. Induction of pulmonary thromboembolism in mice confirmed the prothrombotic nature of GO. Studies using GO and reduced GO (RGO) revealed that charge distribution on the GO surface has a major role in platelet activation.

RESULTS AND DISCUSSION

Characterization of GO and RGO. We prepared single- or few-layer GO sheets in the order of 0.2 to 5 μm, as revealed from surface characterization studies (Supporting Information Figure S1). Bilayer GO sheets were the most prevalent species in chemically exfoliated GO samples. Detailed high-resolution transmission electron microscopy (HR-TEM) was performed to examine crystallinity and quality of GO sheets. A bilayer (two layers of graphene sheets separated by 0.40 $\pm$ 0.02 nm) GO sheet was clearly observed in Supporting Information Figure S1b (denoted in the red region), which was further confirmed by 2D fast Fourier transform (FFT) (inset in the Supporting Information Figure S1b) performed in the region (denoted by

* Address correspondence to ddass@satyam.net.in.

Received for review March 23, 2011 and accepted May 16, 2011.

Published online May 16, 2011
10.1021/nn201092p

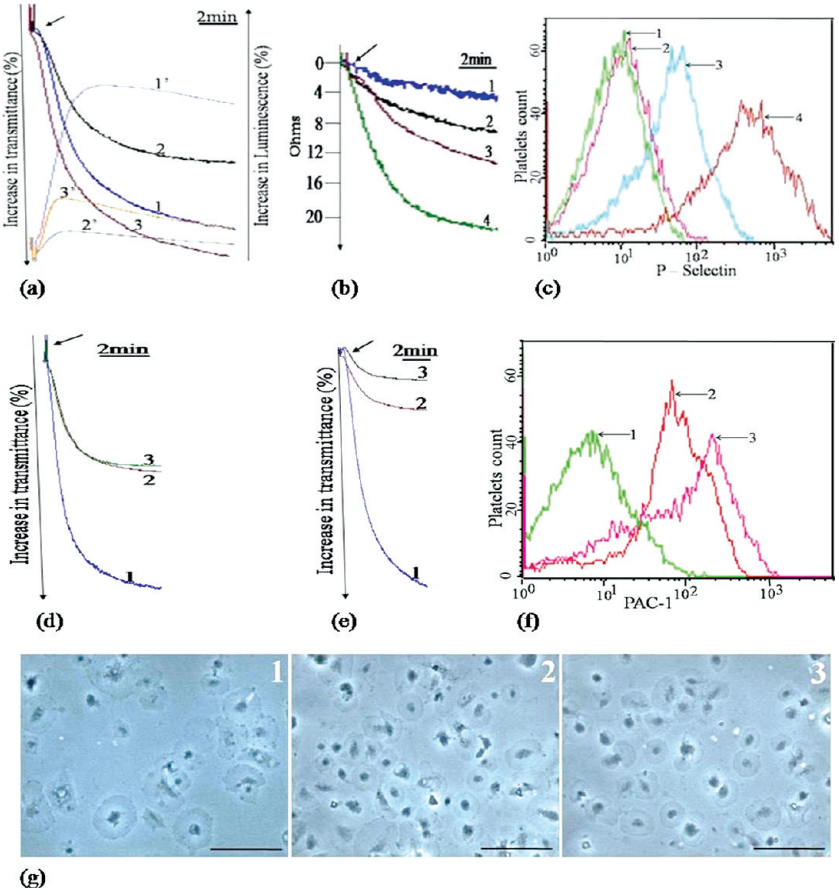

Figure 1. Platelet stimulation by GO and thrombin. (a) Traces 1, 2, and 3 denote aggregation of washed platelets induced by thrombin (1 U/mL), GO (1 μg/mL), and GO (2 μg/mL), respectively. Corresponding platelet dense body secretion is denoted by traces 1′, 2′, and 3′, respectively. (b) Traces 1−4 denote platelet aggregation in whole blood (studied by electronic impedance) in presence of 5, 10, 20, and 25 μg/mL GO, respectively. (c) Flow cytometric analysis of P-selectin exposure in platelets treated with either thrombin or GO: 1, resting platelets; 2, GO (5 μg/mL)-stimulated platelets; 3, GO (20 μg/mL)-stimulated platelets; 4, thrombin (1 U/mL)-activated platelets. (d,e) Aggregation of platelets pretreated with either EGTA (6 mM) (trace 2), RGDS (0.5 mM) (trace 3), or buffer (trace 1), followed by stimulation with either GO (2 μg/mL) (d) or thrombin (1 U/mL) (e). (f) Flow cytometric analysis of PAC-1 binding to platelets: 1, resting platelets; 2, thrombin (1 U/mL)-activated platelets; 3, GO (2 μg/mL)-stimulated platelets. (g) Adhesion and spreading of platelets on immobilized fibrinogen: 1, untreated platelets; 2, GO (2 μg/mL)-treated platelets; 3, thrombin (1 U/mL)-treated platelets. Scale bars = 10 μm. Results shown are representative of five individual experiments.

green square) of Figure S1a. The FFT of a single hexagonal graphene network produces six spots of 0.21 ± 0.05 nm spacing, which corresponds to a single layer.[30] In this case, FFT showed two sets of hexagons (12 spots) directly resembling two-layer graphene sheets. Supporting Information Figure S1d represents a reconstructed image of Supporting Information Figure S1c by filtering in the frequency domain to remove unwanted noise, which clearly reveals a Moiré pattern of bilayer graphene sheets.[30,31] Above observations confirmed perfect crystalline quality of GO sheets in our preparation. FTIR spectra revealed the presence of oxygenated groups in GO and reduced functional groups in RGO (Supporting Information Figure S1e).

Effect of GO on Platelet Functions. Addition of GO to a suspension of freshly isolated human platelets (0.5−0.8 × 10^9 cells/mL) induced cell aggregation upon stirring at 37 °C in a concentration-dependent manner (Figure 1a). At 2 μg/mL, aggregation induced by GO was even stronger than that elicited by thrombin (1 U/mL), one of the most potent platelet agonists. In order to check the effect of GO on human platelets suspended in physiological milieu, aggregation was induced in whole blood and measured by electronic impedance. GO, too, stimulated platelet aggregation in whole blood in a dose-dependent manner (Figure 1b).

Upon activation, platelets recruit additional platelets into the growing thrombus by local release of ADP and thromboxane A2, which stimulate the nearby platelets through potentiation of thrombin action. To check contribution of these agonists in GO-induced platelet aggregation, we preincubated cells with apyrase (10 U/mL), an ADP scavenger, or aspirin (1 mM), inhibitor of cyclooxygenase. Aspirin had no effect upon platelet aggregation induced by GO, while apyrase could attenuate aggregation by only 15 ± 3% (data not shown), thus ruling out significant contribution of these secondary mediators. GO-induced platelet aggregation, however, was significantly attenuated by U73122 (by 87 ± 5%) and Ro-31-8425 (by 80 ± 3%),

specific inhibitors of phospholipase C (PLC) and protein kinase C (PKC), respectively (Supporting Information Figure S2), thus implicating PLC-PKC axis in GO-mediated signaling.

Fibrinogen had to be secreted from platelet granules to establish aggregation of cells suspended in buffer. Therefore, we asked whether platelet aggregation in the presence of GO was associated with release of contents of platelet granules. Secretion of adenine nucleotides by platelets was investigated concomitantly with aggregation as an index of release from platelet dense bodies. Both GO and thrombin induced release of dense granule contents parallel with platelet aggregation (Figure 1a), though the effect of GO on secretion was much weaker than its stimulatory effect on aggregation. Exposure of P-selectin (CD62P) on surface membrane, a marker for release of alpha granule contents, was subsequently studied by flow cytometry using a fluorescently labeled antibody. As expected, thrombin (1 U/mL) showed 8-fold increase in surface expression of P-selectin (Figure 1c, trace 4). However, GO, at higher concentrations (5 and 20 μg/mL), could induce only 0.8 and 9% rise in P-selectin expression, respectively (Figure 1c, traces 2 and 3). Thus, GO was significantly less potent than thrombin in eliciting release from the platelet granules. These observations underscore the existence of different signaling pathways leading to diverse responses in stimulated platelets.[32,33]

Platelet aggregation is based on interaction between cell surface integrins $\alpha_{IIb}\beta_3$ and soluble fibrinogen. Thrombin-induced aggregation was almost completely inhibited (by 90 $\pm$ 5%) by either EGTA, chelator of extracellular Ca^{2+} that dissociates the integrin subunits[34] (Figure 1e, trace 2), or the tetrapeptide Arg-Gly-Asp-Ser (RGDS), competitive inhibitor of fibrinogen binding (Figure 1e, trace 3), validating the contention that thrombin provoked stable fibrinogen–integrin interaction. Intriguingly, EGTA or RGDS could inhibit GO-induced platelet aggregation only to the extent of 50 $\pm$ 3% (Figure 1d), raising the possibility that GO sheets could have agglutinating effect on platelets, which would partially contribute to the overall platelet aggregation observed in the presence of GO. Direct GO–platelet interaction presented in Figure 4, too, supported this contention. This might also explain the major increase in light transmittance induced by GO in the absence of corresponding release from platelet granules unlike the situation with thrombin.

Agonists induce conformational changes in platelet surface integrins $\alpha_{IIb}\beta_3$ (inside-out signaling), rendering them competent for high-affinity binding with fibrinogen. In order to understand whether GO, too, provoked inside-out signaling leading to platelet aggregation, platelets were incubated with monoclonal antibody PAC-1, which selectively recognizes the high-affinity conformation of $\alpha_{IIb}\beta_3$.[35] Exposure to GO (2 μg/mL) significantly augmented PAC-1 binding to platelets (Figure 1f, curves 1 and 3), the extent of which was even higher than that elicited by 1 U/mL thrombin (Figure 1f, curve 2), indicating that GO enhanced fibrinogen binding to platelet integrins.

As GO was found to induce robust aggregatory response partially mediated by soluble fibrinogen, we asked whether it could also modulate interaction of platelets with immobilized fibrinogen. As expected, thrombin-pretreated platelets exhibited enhanced adhesion to fibrinogen (Figure 1g, panel 3). Pretreatment of platelets with GO (2 μg/mL), too, showed almost 2-fold increase in the number of cells adhered onto fibrinogen matrix in all the fields examined (Figure 1g, panel 2), while adhesion to the poly-L-lysine matrix was unaffected by GO treatment (not shown), reflective of enhanced integrin–fibrinogen interaction following exposure to graphene.

Platelet activation is associated with phosphorylation of multiple cytosolic proteins on tyrosine residues.[36] To understand the molecular basis of graphene-induced platelet reactivity, we studied tyrosine phosphoproteome in GO-treated platelets. GO (2 μg/mL) evoked phosphorylation of multiple proteins on tyrosine in both stirred (aggregated) and unstirred platelets, while untreated (resting) cells had only few phosphorylated peptides (Figure 2a, lanes 1, 3, and 4, respectively). Induction of protein phosphorylation in unstirred platelets was consistent with direct effect of GO on platelet signaling independent of integrin $\alpha_{IIb}\beta_3$ engagement. Thrombin (1 U/mL) also stimulated phosphorylation of several proteins on tyrosine (Figure 2a, lane 2), as extensively reported. Interestingly, a 72 kDa protein exhibited significantly higher phosphorylation in the platelets treated with GO, and not with thrombin.

Human platelets express a significant amount of nonreceptor protein tyrosine kinases of the Src family as well as syk kinase, whose activities are upregulated by physiological agonists. In order to implicate individual kinases in tyrosine phosphorylation induced by GO, we preincubated cells with PP2 and piceatannol, specific inhibitors of Src and syk, respectively, or DMSO (vehicle), followed by challenge with GO. Both the inhibitors, PP2 and piceatannol, brought about significant attenuation in GO-mediated global protein phosphorylation by 50 $\pm$ 5 and 43 $\pm$ 2%, respectively (Figure 2b, lanes 3 and 5, respectively) compared to GO-treated platelets (Figure 2b, lane 2), thus linking Src and syk kinase activities with phosphorylation events downstream of GO. PP3, an inactive analogue of PP2, was less effective at inhibiting phosphorylation (Figure 2b, lane 4). In support of these data, we measured expression levels of Src pTyr-529 in GO-treated platelets using a phospho-specific antibody. Src is maintained in an autoinhibited state in resting cells by intramolecular interactions involving pTyr-529

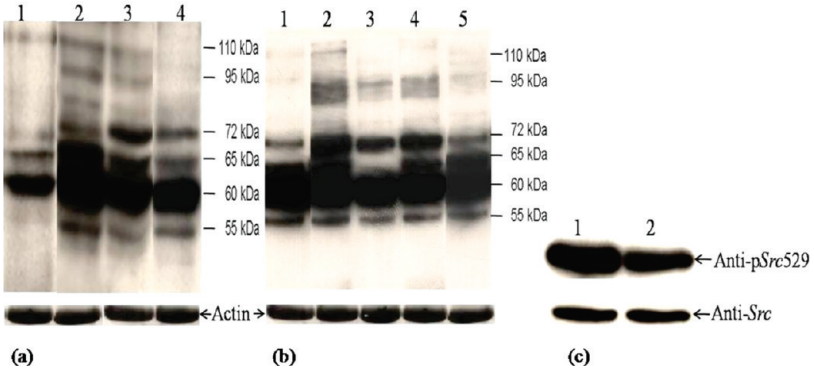

Figure 2. Effect of GO on platelet tyrosine phosphoproteome. (a) GO induces tyrosine phosphorylation in platelet proteins. Lane 1, resting platelets; lane 2, thrombin (1 U/mL)-aggregated platelets; lanes 3 and 4, GO (2 μg/mL)-treated stirred (aggregated) and unstirred platelets, respectively. Lower panel, corresponding Coomassie-stained actin indicative of equal protein loading. (b) Effect of inhibitors of Src and syk on tyrosine phosphoproteome in GO-stimulated platelets. Lane 1, resting platelets; lanes 2−5, GO (2 μg/mL)-treated stirred platelets preincubated with DMSO (lane 2), PP2 (lane 3), PP3 (lane 4), and piceatannol (lane 5). Lower panel, corresponding Coomassie-stained actin indicative of equal protein loading. (c) Src pTyr-529 content in resting (lane 1) and GO (2 μg/mL)-treated platelets (lane 2) studied using a phospho-specific antibody. Lower panel exhibits Src content, indicative of equal protein loading in the lanes. Results shown are representative of four independent experiments.

residue, dephosphorylation of which results in augmentation of kinase activity.[37] We found Src pTyr-529 to be significantly decreased (by 70 ± 5%) in GO-treated platelets as compared to untreated cells (Figure 2c), suggestive of Src stimulation in the presence of GO. However, we did not observe reciprocal changes at Y418, the activating phosphorylation site in Src (not shown).

Ca^{2+} is a critical regulator of intracellular signaling affecting platelet functions. To elucidate underlying molecular details of platelet sensitivity toward GO, we studied the effect of GO on platelet cytosolic Ca^{2+}, $[Ca^{2+}]_i$. GO (2 μg/mL) evoked an initial rise in $[Ca^{2+}]_i$ by more than 5-fold the resting value, followed by plateau (Figure 3a, trace 2), which was similar to the effect of thrombin on platelet intracellular calcium flux (Figure 3a, trace 1). Thrombin is known to mobilize Ca^{2+} from cytosolic stores through the action of inositol trisphosphate (IP_3), which is generated by enzymatic activity of PLCβ. In order to understand the mechanism of GO-mediated rise in platelet $[Ca^{2+}]_i$, we separately pretreated platelets with specific inhibitors of PLC (U73122) or PKC (Ro-31-8425) or 2-aminoethoxydiphenyl borate (2-APB), an IP_3 receptor antagonist. Each of these reagents significantly suppressed GO-induced rise in platelet intracellular calcium (Figure 3b), thus implicating PLC-IP_3/diacylglycerol-Ca^{2+}/PKC axis in signaling triggered by GO. Increase in the level of intracellular cyclic adenosine monophosphate (cAMP) is known to inhibit platelet activation by prohibiting $[Ca^{2+}]_i$ mobilization.[38] To further define signaling parameters regulating GO-induced platelet stimulation, platelets were treated with 5 mM dibutyryl cAMP, a membrane-permeable nonhydrolyzable analogue of cAMP. Dibutyryl cAMP significantly inhibited (75 ± 5%) GO-induced platelet aggregation (Figure 3c), implicating a regulatory role of cAMP in graphene signaling similar to thrombin.

As reactive oxygen species (ROS) have a central role in platelet signaling,[39] we asked whether GO could elicit generation of ROS in platelets. H_2DCF/DA (20 μM)-loaded platelets were exposed to different concentrations of GO at 37 °C for 10 min, and changes in fluorescence were recorded. The results showed a dose-dependent increase in fluorescence intensity induced by GO (Figure 3d), consistent with stimulation of ROS production. At high concentration (20 μg/mL), GO elevated platelet cytosolic ROS to a level comparable to that achieved with H_2O_2 (10 μM), which was completely scavenged by the reductant *N*-acetylcysteine (NAC) (Figure 3d).

Platelet activation by physiological agonists like thrombin is associated with extensive reorganization of actin-based cytoskeleton. In order to find out whether GO could modulate platelet cytoskeleton, polymerized actin content was evaluated in platelets labeled with phalloidin-FITC. Thrombin (1 U/mL) and GO (2 μg/mL) evoked 13 ± 0.8 and 11 ± 0.5% rise in the content of filamentous (F)-actin, respectively (Supporting Information Figure S3, trace 2). Pretreatment with cytochalasin D, a barbed end blocking agent, precluded actin filament formation induced by thrombin but not by GO (Supporting Information Figure S3, trace 3), suggestive of polymerization of actin at pointed ends of filaments in GO-treated platelets.

We subsequently explored possible toxic effects of GO by examining leakage of lactate dehydrogenase (LDH) from platelets. GO (5−20 μg/mL) did not elicit significant release of LDH from platelet cytosol (Supporting Information Figure S4a), thus ruling out breach in membrane integrity. On the contrary, exposure of platelets to the detergent digitonin (30 μM) brought about extrusion of more than 90% of LDH. To further characterize the effect of GO on platelet membrane, we studied affinity of 1-anilino-8-naphthalene

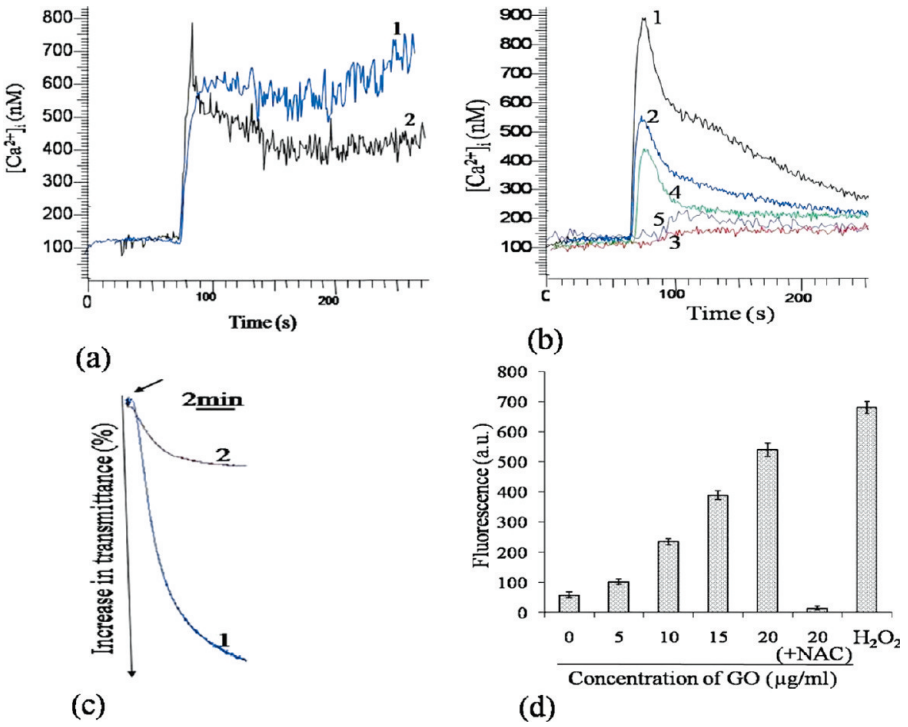

Figure 3. Molecular regulators of GO-mediated platelet signaling. (a) Intracellular calcium flux in thrombin- and GO-stimulated platelets. Fura-2-loaded platelets were treated either with thrombin (1 U/mL) (trace 1) or with GO (2 μg/mL) (trace 2) in the presence of extracellular calcium (1 mM). (b) GO-induced rise in intracellular calcium in platelets pretreated with U73122 (10 μM, trace 2; 20 μM, trace 3), APB (5 μM, trace 4), Ro-31-8425 (5 μM, trace 5), or vehicle (trace 1) in the presence of EGTA (2 mM). (c) Effect of dibutyryl cAMP (5 mM) on GO (2 μg/mL)-induced platelet aggregation. Traces 1 and 2 denote aggregation in the absence and presence of dibutyryl cyclic AMP, respectively. (d) GO increased ROS generation in platelets in a concentration-dependent manner. H_2DCF-loaded platelets (control as well as GO-treated) were treated with different concentrations of GO, H_2O_2 (10 μM), and NAC (1 μM), as indicated. Fluorescence was recorded at 530 nm (excitation, 500 nm). The result was representative of five independent experiments (mean $\pm$ SD).

sulfonate (ANS), an anionic fluorescent probe, toward the platelet membrane. Upon binding, the emission peak of ANS was blue-shifted from 520 to 480 nm accompanied by intensity enhancement. Pretreatment of platelets with GO (1 and 2 μg/mL) had no effect on ANS fluorescence intensity. However, exposure to higher concentrations of GO (5, 10, and 20 μg/mL) was associated with significant decrease in ANS fluorescence (Supporting Information Figure S4b), suggestive of alteration in platelet membrane disorder or surface charge at higher concentrations of GO.

Next, we examined mitochondrial transmembrane potential ($\Delta\psi_m$) by flow cytometry in GO-treated platelets labeled with JC-1. Lowered fluorescence ratio (FL2/FL1) is consistent with collapse of $\Delta\psi_m$ during apoptosis. GO, at concentrations up to 2 μg/mL, had no effect on JC-1 FL2/FL1 ratio. However, the ratio dropped progressively and significantly with increase in the concentration of GO (5−20 μg/mL) (Supporting Information Figure S4c). As expected, the protonophore, carbonyl cyanide 3-chlorophenylhydrazone (CCCP), brought about significant collapse of $\Delta\psi_m$ to the level achieved with 20 μg/mL GO (Supporting Information Figure S4c). These observations were consistent with induction of apoptosis in platelets upon exposure to high concentration of GO in the absence of evidence of necrosis (no breach in membrane integrity). Thus, GO behaves like physiological agonists, which have been shown to stimulate apoptotic events in platelets.[40]

We have recently reported that the population of GO can be characterized by flow cytometry based on optical scattering and fluorescence properties of individual GO sheets.[41] GO is endowed with intrinsic fluorescence, eliciting strong signal in the FL3 channel of the flow cytometer, with no detectable fluorescence in FL4 (Figure 4a). In order to illustrate interaction between GO sheets and platelets, we labeled platelets with allophycocyanin (APC)-conjugated anti-CD41a antibody, which emanated robust signal in FL4 while nil in FL3 channel (Figure 4b). FL3 and FL4 parameters of GO and platelet population were acquired in the dot plot acquisition quadrants. When GO (5 μg/mL) was co-incubated with APC-labeled platelets (0.5×10^8/mL) at room temperature for 10 min, the majority of events shifted to the upper right quadrant (from almost nil to 70%) (Figure 4c), suggestive of profound physical interaction between GO sheets and platelets. However, nearly 30% events still stayed behind in the upper left quadrant (Figure 4c), which represented free GO sheets. We could induce the remaining GO population to form a complex with platelets by adding increments

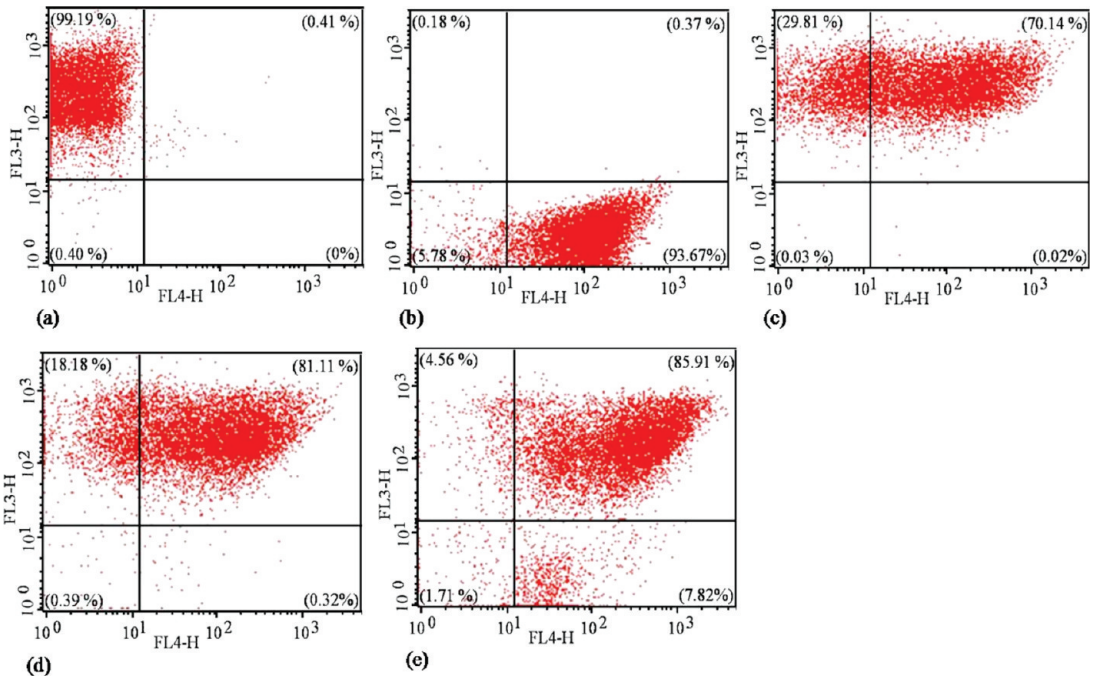

Figure 4. FL3−FL4 parameters in dot plot acquisition quadrants showing GO−platelet interactions: (a) GO population; (b) APC-labeled platelets; (c−e) co-incubation of GO (5 μg/mL) with different dilutions of APC-labeled platelets (0.5, 1, and 2 × 10^8/mL, respectively). The number of events analyzed for each population was 10 000. The number within parentheses in each quadrant represents percentage of total gated events in the respective quadrant. The results were representative of five independent experiments.

of cells into the incubation mixture, which resulted in progressive decline in the events in upper left quadrant and concomitant rise in signal in the upper right quadrant (Figure 4d,e).

There have been recent reports suggesting correlation between the degree of functionalization of carbon nanotubes and the ensuing cytotoxic effects.[42,43] Surface topography of nanocarbon substrates is shown to have profound influence on their interface with live cells.[44] In support of this, GO sheets having small sizes (10−30 nm) and coated with a biocompatible polymer like polyethylene glycol had no obvious toxicity when administered in mice,[45] while as-prepared GO in the absence of further coating led to serious accumulation in lungs and pulmonary toxicity.[46] In order to investigate if graphene functionalization, too, impacted its interaction with cells, we studied the effect of RGO on platelets. RGO (2 μg/mL) elicited a minor aggregatory response, which was about 10% of that induced by GO at the same concentration (Figure 5a). Even a much higher concentration of RGO (10 μg/mL) could evoke only 20% aggregation (Figure 5a), indicating a significant role of graphene surface functionalization (charge distribution) in platelet stimulation.

Next we studied the effects of GO and RGO on ultrastructural details of platelets. Scanning electron microscopy showed resting platelets as spherical cells of 2−3 μm diameter, which remained separated from each other (Figure 5b, panel 1). Strongly contrasting these GO-treated platelets exhibited well-developed hyaloplasmic processes (pseudopods), which connected the cells forming large clumps (aggregates) (Figure 5b, panel 2). Platelets pretreated with RGO appeared similar to the resting cells, but the presence of small hyaloplasmic extensions indicated weak activation of these platelets (Figure 5b, panel 3). As expected, thrombin-treated platelets exhibited "strong activation" phenotype, which closely resembled the GO-treated cells (Figure 5b, panel 4).

Under a transmission electron microscope, untreated platelets were characterized by centrally localized granules and scattered vacuoles (Figure 5c, panel 1). GO-treated platelets exhibited more prominent hyaloplasmic extensions and less scattered granules, consistent with stronger activation of cells (Figure 5c, panel 2). Contrasting this, in RGO-pretreated platelets, most of the granular and vacuolar spaces were retained with fewer hyaloplasmic processes, indicative of weaker stimulation of the cells (Figure 5c, panel 3). Thrombin-activated platelets (Figure 5c, panel 4) showed characteristic well-developed hyaloplasmic processes, highly scattered dense granules, and constricted vacuolar spaces.

As the above series of *in vitro* studies were consistent with GO being a potent activator of platelets, we asked next whether GO could induce thrombus formation in an *in vivo* thrombosis model upon access into the circulatory system of the organism. GO (250 μg/kg body weight), RGO (250 μg/kg body weight), or collagen−epinephrine mixture (as positive control) was injected intravenously into different groups of mice,

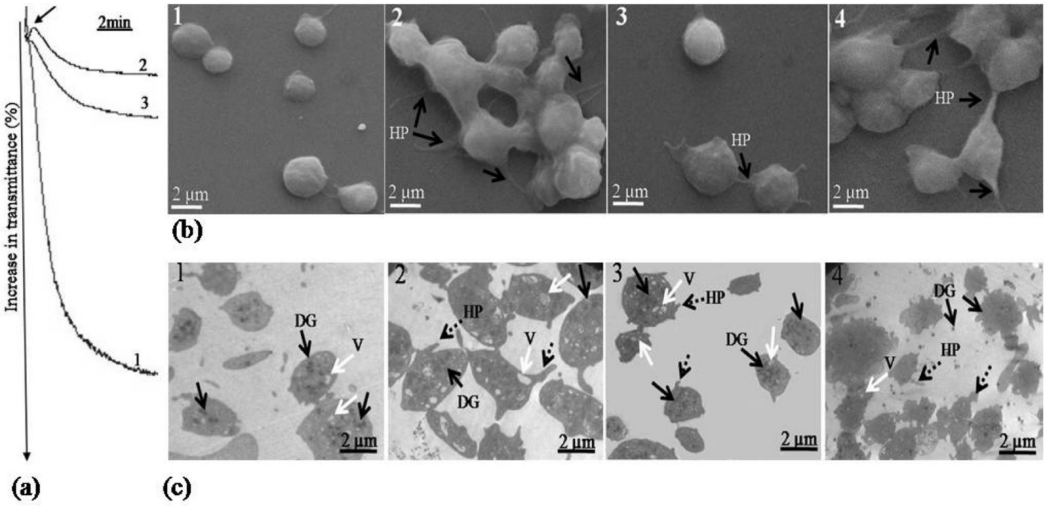

Figure 5. Differential effects of GO and RGO on human platelets. (a) Effect of RGO on platelet aggregation. Traces 1, 2, and 3 denote aggregation of platelets induced by GO (2 μg/mL) and RGO (2 and 10 μg/mL), respectively. The data are representative of five different experiments. (b) Scanning electron micrographs of platelets: 1, resting platelets; 2, GO (2 μg/mL)-treated platelets; 3, RGO (2 μg/mL)-treated platelets; 4, thrombin (1 U/mL)-activated platelets; HP, hyaloplasmic processes. (c) Transmission electron micrographs through sections of platelets. Details of panels 1−4 are the same as those in panel b. DG, dense granules; V, vacuoles; HP, hyaloplasmic processes.

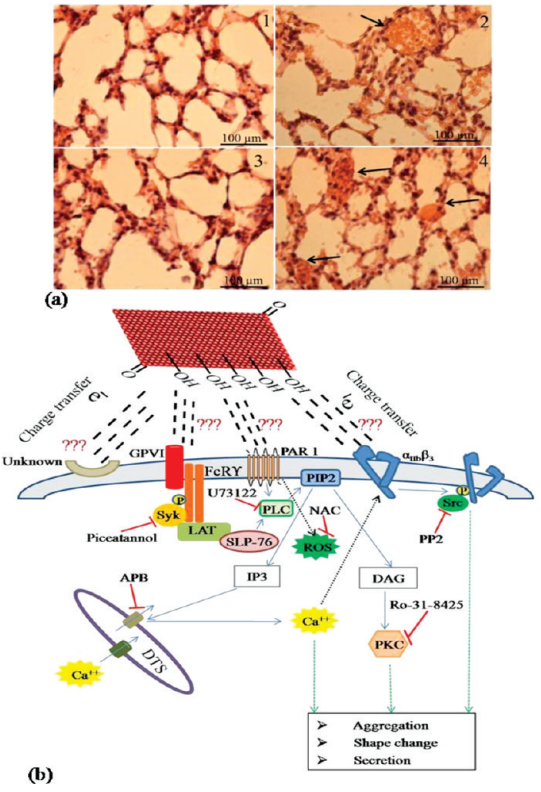

Figure 6. (a) Light microscopy of hematoxylin and eosin stained sections of lungs after intravenous injection of mice with normal saline (panel 1), GO (panel 2), RGO (panel 3), and collagen−epinephrine mixture (panel 4). Arrows indicate platelet-rich thrombi occluding lung vessels. (b) Proposed model based upon current data implicates PLC-IP_3/diacylglycerol-Ca^{2+}/PKC transduction pathway and activity of nonreceptor protein tyrosine kinases, Src and syk, in GO-induced platelet activation. Surface charges on GO might contribute to stimulation of platelet signaling through an unknown mechanism.

and histological sections of lungs were obtained after 15 min. Hematoxylin-eosin stained sections showed significantly higher number of lung vessels (48 and 64%) to be totally or partially occluded by platelet thrombi in mice administered with GO or collagen−epinephrine mixture, respectively, compared to the control (saline-treated) mice. RGO administration elicited significantly less occlusion of vessels (8%) in lungs, which contrasted the case with GO (Figure 6a). These results are consistent with a surface charge-dependent induction of thromboembolism *in vivo* by GO.

CONCLUSION

In summary, with the rapid surge in research and development activities on carbon-based nanomaterials, risk associated with them is a reason for serious concern among the scientific community. Toxicity of carbon nanotubes has already been extensively reported. Thus, it is imperative that every carbon-based nanomaterial should be critically scrutinized for its effect on a living system. Graphene is the newest nanocarbon with enormous potential for biomedical applications. In this report, we have analyzed interaction between graphene oxide and blood platelets, the cells responsible for acute arterial thrombotic events like ischemic heart disease and stroke. Our studies demonstrate that GO can evoke strong aggregatory response in platelets in a scale comparable to that elicited by thrombin, one of the most potent physiological agonists of platelets. GO-induced platelet activation could be attributed to release of intracellular free calcium from cytosolic stores and activation of nonreceptor protein tyrosine kinases of the Src family in platelets (Figure 6b). When administered

intravenously into mouse, GO triggered extensive pulmonary thromboembolism, consistent with the highly potent thrombogenic nature of GO. Significantly, RGO was much less effective in activating platelets, which may be correlated with reduced charge density on graphene surface. In conclusion, future biomedical applications of GO as a therapeutic or diagnostic tool should be critically evaluated against its serious thrombogenic threat.

METHODS

Synthesis of GO and RGO. GO sheets were prepared by refluxing commercially obtained graphite powder (5 g, Sigma-Aldrich) in strongly acidic mixture of sulfuric acid (87.5 mL) and nitric acid (45 mL). After graphite powder was well dispersed, potassium chlorate (55 g) was added slowly over 15 min to avoid sudden increase in temperature. The reaction flask was loosely capped to allow evolution of gas from the reaction mixture and was stirred for 5 days at room temperature. On completion of the reaction, the mixture was poured into 4 L of deionized water and filtered. The residue (GO) was washed repeatedly with deionized water until the pH of the filtrate was neutral. The GO slurry was then freeze-dried and stored in the vacuum oven at 60 °C until use. The graphene sheets so obtained were well-functionalized with carbonyl and hydroxyl groups, which were responsible for the colloidal nature of GO in aqueous solution. The details of characterization of GO are described elsewhere.[41] For preparation of RGO, the freeze-dried GO was charged into a quartz tube and purged with argon for 30 s. Rapid thermal heating (>2000 °C/min) to 1100 °C reduced functional epoxy and hydroxyl groups from the surface of GO sheets through evolution of CO_2. The release of CO_2 inevitably leaves behind vacancies and some residual functional sites that are responsible for the colloidal nature of RGO sheets in the water solutions.[47]

Platelet Preparation. Platelets were isolated by differential centrifugation from fresh human blood, as already described.[48] Briefly, blood from healthy volunteers was collected in citrate-phosphate-dextrose adenine and centrifuged at 180*g* for 20 min. PRP (platelet-rich plasma) was incubated with 1 mM acetylsalicylic acid for 15 min at 37 °C. After addition of ethylenediaminetetraacetic acid (EDTA) (5 mM), platelets were sedimented by centrifugation at 800*g* for 10 min. Cells were washed in buffer A (20 mM HEPES, 138 mM NaCl, 2.9 mM KCl, 1 mM $MgCl_2$, 0.36 mM NaH_2PO_4, 1 mM EGTA (ethylene glycol tetraacetic acid), supplemented with 5 mM glucose and 0.6 ADPase units of apyrase/mL, pH 6.2). Platelets were finally resuspended in buffer B (pH 7.4), which was the same as buffer A but without EGTA and apyrase. The final cell count was adjusted to $0.5-0.8 \times 10^9$/mL. Morphology of the cells was studied under a fluorescence microscope with phase contrast attachment (Nikon model Eclipse Ti-E, Towa Optics, India). All steps were carried out under sterile conditions, and precautions were taken to maintain the cells in an inactivated state.

Platelet Aggregation and Secretion Studies. Platelets were stirred (1200 rpm) at 37 °C in a whole blood/optical Lumi-Aggregometer (Chrono-log model 700-2, Wheecon Instruments, India) for 1 min prior to the addition of GO or the agonists. Aggregation was measured as percent change in light transmission, where 100% refers to transmittance through a blank sample. ATP secretion was measured with Chronolume reagent (stock concentration, 0.2 μM luciferase/luciferin). Luminescence generated by platelet-secreted ATP was monitored using Lumi-Aggregometer in parallel with aggregation measurement. Finally, cells were boiled in Laemmli lysis buffer and stored at −20 °C until further analysis.

Platelet Adhesion Study. To study platelet adhesion to an immobilized matrix, control cells as well as cells pretreated with GO or thrombin were fixed with 4% paraformaldehyde. Cells were charged onto slides coated either with poly-L-lysine (0.01% w/v) or fibrinogen (100 μg/mL), incubated for 30 min at room temperature followed by washing. The adhered cells were observed under a fluorescence microscope with phase contrast attachment (Leica model DM LB2, Labindia Instruments) at 100× in oil. Time-lapse events were captured by Leica DFC 320 CCD camera using IM50 software (Leica) and analyzed by NIS-Elements AR imaging software (Nikon, Towa Optics, India).

Measurement of PAC-1 Binding. Platelets (2×10^8 cells in 200 μL) were incubated at 37 °C for 10 min without stirring in the presence of either thrombin or GO, followed by addition of equal amounts of 4% paraformaldehyde for 30 min. Cells were washed and resuspended in PBS and incubated with 10 μL of FITC-labeled PAC-1 antibody against active conformation of $\alpha_{IIb}\beta_3$ for 30 min in the dark at room temperature. Samples were again washed and analyzed with a FACSCalibur flow cytometer (Becton Dickinson India Pvt. Ltd., Gurgaon). Forward and side scatter voltages were set at E00 and 273, respectively, with a threshold of 52 V. An amorphous region (gate) was drawn to encompass the platelets to differentiate from noise and multiplatelet particles. After compensation for FITC and PE, all fluorescence data were collected using four-quadrant logarithmic amplification. CD61-positive 10 000 events were collected for each sample. The increase in PAC-1 binding was calculated measuring the difference in mean fluorescence intensity between the stimulated and unstimulated samples using CellQuest Pro software.

Surface Expression of P-Selectin. Platelets were processed as described in the earlier paragraph, incubated with 5 μL of PE-labeled antibody against P-selectin (CD62P) and analyzed by flow cytometry.

Measurement of F-Actin Content in Platelets. The F-actin contents of resting and activated cells, with and without prior treatment with cytochalasin D (10 μM), were determined from the extent of phalloidin-FITC staining. Cells were fixed with equal volume of 4% paraformaldehyde at 37 °C for 30 min, followed by permeabilization at room temperature for 60 min in the presence of 0.1% Triton-X-100 containing 10 μM phalloidin-FITC in the dark. Fluorescence was analyzed with the flow cytometer.

Determination of Mitochondrial Transmembrane Potential. Mitochondrial transmembrane potential ($\Delta\psi$) was measured using the potential-sensitive fluorochrome JC-1, which is capable of selectively entering into mitochondria upon membrane polarization and form JC-1 aggregates (red). As the membrane potential collapses, color changes from red to green due to dye monomerization. To examine mitochondrial transmembrane potential, we incubated control platelets and platelets treated either with GO (1 to 20 μg/mL) or CCCP (10 μM) with 10 μM JC-1 for 15 min at 37 °C in the dark. Cells were washed in PBS, and JC-1 fluorescence was analyzed on FL1 and FL2 channels of the flow cytometer for the detection of the dye monomer and *J*-aggregates, respectively. The ratio between red/green (FL2/FL1) fluorescence reflected mitochondrial transmembrane potential, whereas co-treatment with the protonophore CCCP resulted in decreased JC-1 fluorescence ratio and served as a positive control for disruption of mitochondrial transmembrane potential.

Immunoblotting Studies. Platelet proteins were separated on 10% SDS-PAGE (sodium dodecyl sulfate polyacrylamide gel electrophoresis) gels and electrophoretically transferred to polyvinylidene fluoride (PVDF) membrane by using TE 77 PWR semidry system (GE Healthcare India). Membranes were blocked with 5% bovine serum albumin in 10 mM Tris-HCl, 150 mM NaCl, pH 8.0 (TBS) containing 0.05% Tween-20 for 1 h at room temperature. Blots were incubated overnight with monoclonal antibodies against phosphotyrosine (clone 4G10) (1 μg/mL) or Src (1 μg/mL) and with polyclonal antibody against Src pTyr-529 (1 μg/mL), followed by HRP-labeled antimouse IgG (for antiphosphotyrosine and anti-Src antibodies) or anti-rabbit IgG (for antiphospho-Src antibody) for 2 h in 1:10 000 dilutions from a 1 mg/mL of each antibody stock solution. Antibody binding was detected using enhanced chemiluminescence

and quantified in an Agfa Duoscan T1200 flatbed scanner using GeneTools software (Syngene India Private Ltd.).

Measurement of Intracellular Free Calcium. PRP was incubated with 2 μM Fura-2 AM for 45 min at 37 °C in the dark. Fura-2-loaded platelets were washed and resuspended in buffer B at 1×10^8 cells/mL. Fluorescence was recorded in 400 μL aliquots of platelet suspensions, both resting as well as activated with thrombin (1 U/mL) or GO (2 μg/mL), at 37 °C under nonstirring conditions using a fluorescence spectrophotometer (Hitachi model F-2500, Techcomp India). Excitation wavelengths were 340 and 380 nm, and emission wavelength was set at 510 nm. Changes in intracellular free calcium concentration, $[Ca^{2+}]_i$, upon addition of thrombin (1 U/mL) or GO (2 μg/mL) were monitored from the fluorescence ratio (340/380) using Intracellular Cation Measurement Program in FL Solutions software. Intracellular free calcium was calibrated according to the derivation of Grynkiewicz *et al.*[49]

ANS Binding. Effect of GO (2−20 μg/mL) on platelet membrane microenvironment was studied by labeling the cells with ANS. Labeling was carried out by adding the probe (5 μM final concentration) to the platelet suspension (0.5×10^8/mL) at room temperature. Fluorescence emission spectra were recorded at 37 °C at an excitation of 380 nm using FL Solutions software.

Measurement of LDH Leakage. Control platelets and platelets treated either with GO (5−20 μg/mL) or with digitonin (30 μM) were pelleted by centrifugation at 800*g* for 10 min. Supernatants were preserved, and pellets were resuspended in identical volume of buffer B, followed by sonication. Reaction was initiated by addition of platelet supernatant or sonicate (40 μL) to 500 μL reaction mixtures containing 0.168 mM NADH and 32.52 mM sodium pyruvate at 30 °C. LDH activity was assayed from time course of decrease in NADH absorbance at 340 nm.

Measurement of Intracellular ROS. H_2DCF-DA, a ROS-sensitive probe, was used to detect oxidative activity in platelets. H_2DCF-DA is known to passively diffuse into cells, where its acetate groups are cleaved by intracellular esterases, releasing the corresponding dichlorodihydrofluorescein (DCF) derivative. Subsequent oxidation by intracellular ROS yields a fluorescent adduct that is trapped inside the cell. Aliquots of platelet suspension (1×10^7 cells/mL) were incubated with 20 μM H_2DCF-DA at 37 °C for 30 min. GO (5−20 μg/mL) was added to platelet suspensions 20 min after addition of H_2DCFDA. Fluorescence was measured with a fluorescence microplate reader (BioTek model FLx800, Medispec India) at 37 °C (excitation, 500 nm; emission, 530 nm). Hydrogen peroxide (10 μM) was added to the platelet suspension as a positive control.

Electron Microscopy. Different platelet samples, either with or without GO pretreatment, were fixed in Karnovsky fixative followed by postfixation in osmium tetroxide (1% solution) and dehydrated in ascending grades of acetone. For SEM, dehydrated samples were critical point dried followed by mounting on an aluminum stub with adhesive tape and sputter-coated with colloidal gold. Specimens were viewed under a Leo 435 VP scanning electron microscope at an operating voltage of 15 kV. For TEM, blocks were prepared as previously described.[50] Ultrathin sections (60−70 nm thick) were made with an ultramicrotome (Leica model EM UC6, Labindia). Sections were contrasted with uranyl acetate and alkaline lead citrate. Specimens were mounted on Formvar-coated grids and viewed under Fei Morgagni 268 (D) digital transmission electron microscope at 120 kV using image analysis software from Soft Imaging System GmbH. The final magnifications were derived from the photo-micrographs and the scale bars determined.

Platelet Pulmonary Thromboembolism. GO-induced pulmonary thromboembolism was performed in 8−12 weeks old Swiss male mice, using a method described previously.[51] In control mice, the thrombotic challenge was generated by rapid intravenous injection of 150 μL mixture collagen (200 μg/mL) plus epinephrine (2 μg/mL) into one of the tail veins. In other cases, GO (250 μg/kg body weight) or RGO (250 μg/kg body weight) was administered intravenously into mice. After 15 min, the animal was sacrificed by an overdose of anesthesia. Lungs were removed, rinsed in cold saline, and fixed immediately in 10% formalin for at least 24 h. Lung histology was performed and was counted by light microscopy in paraffin-embedded sections stained with hematoxylin and eosin.[51] At least 10 fields, at a magnification of 40×, were observed for every specimen.

Statistical Methods. Standard statistical methods were used. Parametric methods (*t* test) were used for evaluation and significance tests were considered significant at *P* less than 0.05 (2-tailed tests). Data are presented as means ± SD of at least four individual experiments.

Acknowledgment. Grants received by D. Dash from the Department of Biotechnology (DBT), Government of India, and Indian Council of Medical Research (ICMR), and the equipment support from the DST Unit on Nanoscience and Technology (DST-UNANST), Banaras Hindu University (BHU), are gratefully acknowledged. We sincerely thank Dr. Mohan Kumar, Department of Pathology, IMS, BHU, for helping with the lung histology study and Diwakar Sharma (B. D. India Pvt. Ltd., Gurgaon) for necessary help. Electron microscopy was carried out at SAIF (DST), AIIMS, New Delhi. M.K.S. would like to thank the Ciencia 2007 Program, Foundation of Science and Technology (FCT-Portugal) and facility RNME-Pole University of Aveiro. S.K.S. and S.K. are recipients of research fellowships from the University Grants Commission, New Delhi, and Council of Scientific and Industrial Research, New Delhi, respectively.

Supporting Information Available: Materials used, GO characterization, role of PLC-PKC axis in GO-induced platelet aggregation, effect of GO on platelet F-actin content, membrane integrity figure and their legends. This material is available free of charge *via* the Internet at http://pubs.acs.org.

REFERENCES AND NOTES

1. Zhou, Y.; Yang, H.; Chen, H. Y. Direct Electrochemistry and Reagentless Biosensing of Glucose Oxidase Immobilized on Chitosan Wrapped Single-walled Carbon Nanotubes. *Talanta* **2008**, *76*, 419–423.
2. Kam, N. W. S.; O'Connell, M.; Wisdom, J. A.; Dai, H. J. Carbon Nanotubes as Multifunctional Biological Transporters and Near-Infrared Agents for Selective Cancer Cell Destruction. *Proc. Natl. Acad. Sci. U.S.A.* **2005**, *102*, 11600–11605.
3. Krueger, A. Diamond Nanoparticles: Jewels for Chemistry and Physics. *Adv. Mater.* **2008**, *14*, 2445–2449.
4. Holt, K. B. Diamond at the Nanoscale: Applications of Diamond Nanoparticles from Cellular Biomarkers to Quantum Computing. *Phil. Trans. R. Soc. A* **2007**, *365*, 2845–2861.
5. Huang, H.; Pierstorff, E.; Osawa, E.; Ho, D. Active Nanodiamond Hydrogels for Chemotherapeutic Delivery. *Nano Lett.* **2007**, *7*, 3305–3314.
6. Liu, Z.; Robinson, J. T.; Sun, X.; Dai, H. PEGylated Nano-Graphene Oxide for Delivery of Water Insoluble Cancer Drugs. *J. Am. Chem. Soc.* **2008**, *130*, 10876–10877.
7. Wang, Y.; Li, Y. M.; Tang, L. H.; Lu, J.; Li, J. H. Application of Graphene-Modified Electrode for Selective Detection of Dopamine. *Electrochem. Commun.* **2009**, *11*, 889–892.
8. Kang, X.; Wang, J.; Wu, H.; Aksay, I. A.; Liu, J.; Lin, Y. Glucose Oxidase−Graphene−Chitosan Modified Electrode for Direct Electrochemistry and Glucose Sensing. *Biosens. Bioelectron.* **2009**, *25*, 901–905.
9. Mohanty, N.; Berry, V. Graphene-Based Single-Bacterium Resolution Biodevice and DNA Transistor: Interfacing Graphene Derivatives with Nanoscale and Microscale Biocomponents. *Nano Lett.* **2008**, *8*, 4469–4476.
10. Sun, X.; Liu, Z.; Welsher, K.; Robinson, J. T.; Goodwin, A.; Zaric, S.; Dai, H. Nano-Graphene Oxide for Cellular Imaging and Drug Delivery. *Nano Res.* **2008**, *1*, 203–212.
11. Peng, C.; Hu, W.; Zhou, Y.; Fan, C.; Huang, Q. Intracellular Imaging with a Graphene-Based Fluorescent Probe. *Small* **2010**, *6*, 1686–1692.
12. Hu, W.; Peng, C.; Luo, W.; Lv, M.; Li, X.; Li, D.; Huang, Q.; Fan., C. Graphene-Based Antibacterial Paper. *ACS Nano* **2010**, *4*, 4317–4323.
13. Akhavan, O.; Ghaderi, E. Toxicity of Graphene and Graphene Oxide Nanowalls against Bacteria. *ACS Nano* **2010**, *4*, 5731–5736.
14. Yang, K.; Zhang, S.; Zhang, G.; Sun, X.; Lee, S. T.; Liu, Z. Graphene in Mice: Ultrahigh *In Vivo* Tumor Uptake and Efficient Photothermal Therapy. *Nano Lett.* **2010**, *10*, 3318–3323.

15. Liu, Y.; Yu, D.; Zeng, C.; Miao, Z.; Dai, L. Biocompatible Graphene Oxide-Based Glucose Biosensors. *Langmuir* **2010**, *26*, 6158–6160.
16. Mangum, J. B.; Turpin, E. A.; Antao-Menezes, A.; Cesta, M. F.; Bermudez, E.; Bonner, J. C. Single-Walled Carbon Nanotube (SWCNT)-Induced Interstitial Fibrosis in the Lungs of Rats is Associated with Increased Levels of PDGF mRNA and the Formation of Unique Intercellular Carbon Structures That Bridge Alveolar Macrophages *In Situ*. *Part. Fibre Toxicol.* **2006**, *3*, 1–13.
17. Shvedova, A. A.; Fabisiak, J. P.; Kisin, E. R.; Murray, A. R.; Roberts, J. R.; Tyurina, Y. Y.; Antonini, J. M.; Feng, W. H.; Kommineni, C.; Reynolds, J.; *et al.* Sequential Exposure to Carbon Nanotubes and Bacteria Enhances Pulmonary Inflammation and Infectivity. *Am. J. Respir. Cell Mol. Biol.* **2008**, *38*, 579–590.
18. Warheit, D. B.; Laurence, B. R.; Reed, K. L.; Roach, D. H.; Reynolds, G. A.; Webb, T. R. Comparative Pulmonary Toxicity Assessment of Single-Wall Carbon Nanotubes in Rats. *Toxicol. Sci.* **2004**, *77*, 117–125.
19. Lynch, R. M.; Voy, B. H.; Glass, D. F.; Mahurin, S. M.; Zhao, B.; Hu, H.; Saxton, A. M.; Donnell, R. L.; Cheng, M.-D. Assessing the Pulmonary Toxicity of Single-Walled Carbon Nanohorns. *Nanotoxicology* **2007**, *1*, 157–166.
20. Poland, C. A.; Duffin, R.; Kinloch, I.; Maynard, A.; Wallace, W. A. H.; Seaton, A.; Stone, V.; Brown, S.; Macnee, W.; Donaldson, K. Carbon Nanotubes Introduced into the Abdominal Cavity of Mice Show Asbestos like Pathogenicity in a Pilot Study. *Nat. Nanotechnol.* **2008**, *3*, 423–428.
21. Jia, G.; Wang, H.; Yan, L.; Wang, X.; Pei, R.; Yan, T.; Zhao, Y.; Guo, X. Cytotoxicity of Carbon Nanomaterials: Single-Wall Nanotube, Multi-wall Nanotube, and Fullerene. *Environ. Sci. Technol.* **2005**, *39*, 1378–1383.
22. Muller, J.; Huaux, F.; Moreau, N.; Misson, P.; Heilier, J. F.; Delos, M. Respiratory Toxicity of Multi-wall Carbon Nanotubes. *Toxicol. Appl. Pharmacol.* **2005**, *207*, 221–231.
23. Radomski, A.; Jurasz, P.; Alonso-Escolano, D.; Drews, M.; Morandi, M.; Malinski, T.; Radomski, M. W. Nanoparticle-Induced Platelet Aggregation and Vascular Thrombosis. *Br. J. Pharmacol.* **2005**, *146*, 882–893.
24. Manna, S. K.; Sarkar, S.; Barr, J.; Wise, K.; Barrera, E. V.; Jejelowo, O.; Rice-Ficht, A. C.; Ramesh, G. T. Single-Walled Carbon Nanotube Induces Oxidative Stress and Activates Nuclear Transcription Factor-κB in Human Keratinocytes. *Nano Lett.* **2005**, *5*, 1676–1684.
25. Bihari, P.; Holzer, M.; Praetner, M.; Fent, J .; Lerchenberger, M.; Reichel, C. A.; Rehberg, M.; Lakatos, S.; Krombach, F. Single-Walled Carbon Nanotubes Activate Platelets and Accelerate Thrombus Formation in the Microcirculation. *Toxicology* **2010**, *269*, 148–154.
26. Semberova, J.; Lacerda, S. H. D. P.; Simakova, O.; Holada, K.; Gelderman, M. P.; Simak, J. Carbon Nanotubes Activate Blood Platelets by Inducing Extracellular Ca^{2+} Influx Sensitive to Calcium Entry Inhibitors. *Nano Lett.* **2009**, *9*, 3312–3317.
27. Saller, F.; Schapira, M.; Angelillo-Scherrer, A. Role of Platelet Signaling in Thrombus Stabilization: Potential Therapeutic Implications. *Curr. Signal Transduction Ther.* **2008**, *3*, 22–54.
28. Badruddin, A.; Gorelick, P. B. Antiplatelet Therapy for Prevention of Recurrent Stroke. *Curr. Treat. Options Neurol.* **2009**, *11*, 452–459.
29. Weston, C.; Rao, U. Antiplatelet Drugs in Cardiovascular Diseases. *Int. J. Clin. Pract.* **2003**, *57*, 898–905.
30. Singh, M. K.; Titus, E.; Goncalves, G.; Marques, P. A. A. P.; Bdikin, I; Kholkin, A. L.; Gracio, J. J. A. Atomic-Scale Observation of Rotational Misorientation in Suspended Few-Layer Graphene Sheets. *Nanoscale* **2010**, *2*, 700–708.
31. Miller, D. L.; Kubista, K. D.; Rutter, G. M.; Ruan, M.; Heer, W. A. D.; First, P. N.; Joseph, A. Structural Analysis of Multilayer Graphene *via* Atomic Moiré Interferometry. *Phys. Rev. B* **2010**, *81*, 125427–125432.
32. Charo, I. F.; Feinman, R. D.; Detwiler, T. C.; Smith, J. B.; Ingerman, C. M.; Silver, M. J. Prostaglandin Endoperoxides and Thromboxane A_2 Can Induce Platelets Aggregations in the Absence of Secretion. *Nature* **1977**, *269*, 66–69.
33. Pula, G.; Schuh, K.; Nakayama, K.; Nakayama, K. I.; Walter, U.; Poole, A. W. PKC Regulates Collagen-Induced Platelet Aggregation through Inhibition of VASP-Mediated Filopodia Formation. *Blood* **2006**, *108*, 4035–4044.
34. White, J. G.; Escolar, G. EDTA-Induced Changes in Platelet Structure and Function: Adhesion and Spreading. *Platelets* **2000**, *11*, 56–61.
35. Shattil, S. J.; Hoxie, J. A.; Cunningham, M.; Brass, L. F. Changes in the Platelet Membrane Glycoprotein IIb IIIa Complex During Platelet Activation. *J. Biol. Chem.* **1985**, *260*, 11107–11114.
36. Golden, A.; Brugge, J. S.; Shattil, S. J. Role of Platelet Membrane Glycoprotein IIb-IIIa in Agonist-Induced Tyrosine Phosphorylation of Platelet Proteins. *J. Cell Biol.* **1990**, *111*, 3117–3127.
37. Obergfell, A.; Eto, K.; Mocsai, A.; Buensuceso, C.; Moores, S. L.; Brugge, J. S.; Lowell, C. A.; Shattil., S. J. Coordinate Interactions of Csk, Src, and Syk Kinases with $\alpha_{IIb}\beta_3$ Initiate Integrin Signaling to the Cytoskeleton. *J. Cell Biol.* **2002**, *157*, 265–275.
38. Soslau, G.; McKenzie, R. J.; Brodsky, I.; Devlin, T. M. Extracellular ATP Inhibits Agonist-Induced Mobilization of Internal Calcium in Human Platelets. *Biochim. Biophys. Acta* **1995**, *1268*, 73–80.
39. Krotz, F.; Sohn, H. Y.; Pohl, U. Reactive Oxygen species: Players in the Platelet Game. *Arterioscler. Thromb. Vasc. Biol.* **2004**, *24*, 1988–1996.
40. Lin, K. H.; Chang, H. C.; Lu, W. J.; Jayakumar, T.; Chou, H. C.; Fong, T. H.; Hsiao, G.; Sheu, J. R. Comparison of the Relative Activities of Inducing Platelet Apoptosis Stimulated by Various Platelet-Activating Agents. *Platelets* **2009**, *20*, 575–581.
41. Singh, S. K.; Singh, M. K.; Nayak, M. K.; Kumari, S.; Grácio, J. J. A.; Dash, D. Size Distribution Analysis and Physical/Fluorescence Characterization of Graphene Oxide Sheets by Flow Cytometry. *Carbon* **2011**, *49*, 684–692.
42. Magrez, A.; Kasas, S.; Salicio, V.; Pasquier, N.; Seo, J. W.; Celio, M.; Catsicas, S.; Schwaller, B.; Forro, L. Cellular Toxicity of Carbon-Based Nanomaterials. *Nano Lett.* **2006**, *6*, 1121–1125.
43. Sayes, C. M.; Liang, F.; Hudson, J. L.; Mendez, J.; Guo, W.; Beach, J. M.; Moore, V. C.; Doyle, C. D.; West, J. L.; Billups, W. E.; *et al.* Functionalization Density Dependence of Single-Walled Carbon Nanotubes Cytotoxicity *In Vitro*. *Toxicol. Lett.* **2006**, *161*, 135–142.
44. Agarwal, S.; Zhou, X.; Ye, F.; He, Q.; Chen, G. C. K.; Soo, J.; Boey, F.; Zhang, H.; Chen, P. Interfacing Live Cells with Nanocarbon Substrates. *Langmuir* **2010**, *26*, 2244–2247.
45. Yang, K.; Wan, J.; Zhang, S.; Zhang, Y.; Lee, S.-T.; Liu, Z. *In Vivo* Pharmacokinetics, Long-Term Biodistribution, and Toxicology of PEGylated Graphene in Mice. *ACS Nano* **2011**, *5*, 516–522.
46. Zhang, X.; Yin, J.; Peng, C.; Hu, W.; Zhu, Z.; Li, W.; Fan, C.; Huan, Q. Distribution and Biocompatibility Studies of Graphene Oxide in Mice after Intravenous Administration. *Carbon* **2011**, *49*, 986–995.
47. Schniepp, H. C.; Li, J.; McAllister, M. J.; Sai, H.; Alonso, M. H.; Adamson, D. H.; Prud'homme, R. K.; Car, R.; Saville, D. A.; Aksay, I. A. Functionalized Single Graphene Sheets Derived from Splitting Graphite Oxide. *J. Phys. Chem. B* **2006**, *110*, 8535–8539.
48. Shrivastava, S.; Bera, T.; Singh, S. K.; Singh, G.; Ramachandrarao, P.; Dash, D. Characterization of Novel Anti-Platelet Properties of Silver Nanoparticles. *ACS Nano* **2009**, *3*, 1357–1364.
49. Grynkiewicz, G.; Poenie, M.; Tsien, R. Y. A New Generation of Ca^{2+} Indicators with Greatly Improved Fluorescence Properties. *J. Biol. Chem.* **1985**, *260*, 3440–3450.
50. Dvorak, A. M. Monograph: Procedural Guide to Specimen Handling for the Ultrastructural Pathology Service Laboratory. *J. Electron Microsc. Tech.* **1987**, *6*, 255–301.
51. Momi, S.; Falcinelli, E.; Giannini, S.; Ruggeri, L.; Cecchetti, L.; Corazzi, T.; Libert, C.; Gresele, P. Loss of Matrix Metalloproteinase 2 in Platelets Reduces Arterial Thrombosis *In Vivo*. *J. Exp. Med.* **2009**, *206*, 2365–2379.